Electronic Supplementary Material (ESI) for Journal of Materials Chemistry A.

Atomically Fe doped hollow mesoporous carbon spheres for peroxymonosulfate mediated advanced oxidation process with dual activation pathways

Qing Wang,[a] Xiaomei Liu,[a] An Cai,[a] Hongwei He,[a] Guoliang Zhang,[a] Fengbao Zhang,[a] Xiaobin Fan,[abc] Wenchao Peng[abc] and Yang Li*[abc]

[a]School of Chemical Engineering and Technology, Tianjin University, Tianjin,300354, China. Email: liyang@tju.edu.cn

[b]Haihe Laboratory of Sustainable Chemical Transformations, Tianjin, 300192, China

[c]Institute of Shaoxing, Tianjin University, Zhejiang, 312300, China

Text S1. Experimental Section

Chemicals: $FeCl_3 \cdot 6H_2O$, tetraethoxysilane (TEOS), ammonium hydroxide (NH_4OH, AR, 25–28 wt%), ethanol (AR), hydrofluoric acid (40-45%), methyl phenyl sulfoxide (PMSO), potassium oxalate monohydrate ($K_2C_2O_4.H_2O$), β-carotene were bought from Aladdin Industrial Corporation. Dopamine hydrochloride ($C_8H_{11}NO_2 \cdot HCl$) was bought from Sigma. PMS ($2KHSO_5 \cdot 3KHSO_4 \cdot K_2SO_4$) was obtained from Chemistry. Methanol (MeOH), t-butanol (TBA), furfuryl alcohol (FFA) and benzoquinone (BQ) were obtained from Tianjin Yuanli Chemistry.

Synthesis of Fe-NC HMCS: Typically, 140 mL ethanol, 20 mL H_2O, and 6 mL NH_4OH were stirred together for 5 min at 25 ℃. Then 5.6 mL TEOS was added dropwise into the mixed solution and reacted for 25 min under stirring. Then 160 mL dopamine solution (5 mg mL^{-1}) and 160 mL Fe contained dopamine solution (DA = 5 mg mL^{-1}, Fe = 0.036 μg mL^{-1}) was then added in to the solution alternately. After reacted at room temperature for 12 h, the $SiO_2@Fe^{3+}$-PDA was obtained by centrifugation and washed for several times. The obtained $SiO_2@Fe^{3+}$-PDA was annealed at 800 °C for 5 h in N_2 atmosphere, with a 2 °C·min^{-1} ramping rate. After etching with 5wt% HF solution for 24 h, the inner SiO_2 was removed and Fe-NC HMCS was obtained.

Synthesis of NC HMCS: Typically, the preparation procedure is identical to that of Fe-NC HMCS without the addition of $FeCl_3 \cdot 6H_2O$.

Synthesis of Fe NPs: Typically, the preparation procedure is identical to that of Fe-NC HMCS except the amount of $FeCl_3 \cdot 6H_2O$ was altered to 114 mg.

Synthesis of SiO_2: 5.95 mL tetraethoxysilane (TEOS) was added into 64 ml ethanol

(solution A). 4.2 mL NH_4OH, 94.5 mL ethanol and 30 mL H_2O were mixed together (solution B), and then solution A and solution B were mixed and stirred for 24 h. The suspension was centrifuged, washed with deionized water and ethanol for several times to obtain SiO_2.

Synthesis of Fe/NC non-MCS: Typically, 300 mg SiO_2 was added into 300 mL tris buffer solution (10 mM, pH = 8.5), 600 mg dopamine hydrochloride ($C_8H_{11}NO_2 \cdot HCl$), 4.27 mg $FeCl_3 \cdot 6H_2O$ were subsequently added into the solution and then stirred for 24 h. The suspension was centrifuged, washed with deionized water for several times. The obtained powder was annealed at 800 °C for 5 h in N_2 atmosphere, with a 2 °C·min^{-1} ramping rate. After etching with 5wt% HF solution for 24 h, the inner SiO_2 was removed and Fe/NC non-MCS was obtained.

Synthesis of Fe/NC non-HMCS: Typically, 1.0 g dopamine hydrochloride ($C_8H_{11}NO_2 \cdot HCl$), 7.11g $FeCl_3 \cdot 6H_2O$ were added into 1000 mL H_2O, and then kept stirring for 10 min. 10 mmol Tris was added into the solution and the mixed solution was then stirred for 48 h. The suspension was centrifuged, washed with deionized water for several times. The obtained powder was annealed at 800 °C for 5 h in N_2 atmosphere, with a 2 °C·min^{-1} ramping rate.

Characterization: X-ray diffraction (XRD) patterns were obtained by Bruker Nonius D8 FOCUS X-ray instrument using Cu-Ka radiation. Raman spectra were obtained by Horiba LabRAM HR Evolution with 532 nm laser excitation. X-ray photoelectron spectroscopy (XPS) was recorded by Thermo ESCALAB 250XI spectrometer. The Brunauer–Emmett–Teller (BET) specific surface area was obtained by Bjbuilder SSA-7000 instrument. The morphology of samples is obtained by scanning electron microscopy (SEM, Hitachi S4800) and transmission electron microscopy (TEM, JEM-F200). The aberration-corrected high-angle annular dark-field scanning transmission electron microscopy (AC HAADF-STEM) and X-ray spectroscopy (EDS) mappings were conducted using JEOL JEM-ARM200F STEM/TEM instrument. The ICP-MS

(iCAP6300) was employed to determine the elemental composition of the sample. The local coordination environment of the isolated Fe atoms in the Fe-NC HMCS was detected by Fe K-edge X-ray absorption near edge structure (XANES) and extended X-ray absorption fine structure (EXAFS) spectroscopy. EPR spectra were obtained by Bruker EPR A300 spectrometer.

Peroxymonosulfate Activity test: The degradation experiments were conducted in a 100ml bottle under stirring (500 rpm) at room temperature (25 ℃). BPA was selected as model contaminant. Specifically, 5 mg catalysts were added into a 100ml solution containing BPA (20 ppm) and the mixture were homogeneously dispersed by ultrasonication. Then 30 mg peroxymonosulfate (PMS) was spiked into the solution to start the degradation reaction. At a certain interval, 0.5 mL solution was withdrawn and mixed with 0.5 mL methanol, then solution was filtrated using 0.22 μm membrane to remove the catalysts. The obtained filtrate was subsequently analyzed by high performance liquid chromatography (HPLC, Thermo UltiMate 3000 RSLCnano System). For quenching text, methanol (MeOH), t-butanol (TBA), furfuryl alcohol (FFA), p-benzoquinone (p-BQ), β-carotene, methyl phenyl sulfoxide (PMSO) were introduced into the solution before the peroxymonosulfate (PMS) was added. For stability test, the used catalysts were washed with deionized water and alcohol after each cycle. Electrochemical measurements were carried out by three-electrode system using a CHI760E electrochemical workstation. 5 mg catalysts were dissolved into 475 μL ethanol, 475 μL water. After that, 50 μL of Nafion solution was added into the mixed solution followed by sonication for 30 min. 5 μL mixture was dropped onto the surface of GCE. The catalysts loaded GCE, Ag/AgCl and Pt electrodes were chosen as working, reference and counter electrodes, respectively. The PMS and BPA were sequentially added into the solution to monitor the change of open circuit potentials (OCP) The final concentrations of BPA and PMS were 10 ppm and 1g/L.

Text S2. Density functional theory (DFT) calculations

The models were computed with density functional theory (DFT) using projected augment wave method as implemented in the Vienna ab initio Simulation Package (VASP) code[1, 2]. The generalized gradient approximation (GGA) of Perdew-Burke-Ernzerhof (PBE) is used for the exchange-correlation potential[3]. Plane-wave basis set was used with an energy cutoff of 500 eV. The convergence criterion for electronic structure iteration was set to be 1×10^{-5} eV and structural optimization would be terminated until all forces were smaller than 0.02 eV/Å. Polarization effect was considered. The charge transfer was analyzed by calculating the charge density using the Bader charge analysis method[4]. A 15 Å vacuum space was introduced to avoid interactions between adjacent layers, k-mesh was set as 1×1×1 in this work. The adsorption energy was defined as:

$$E_{ads} = E_{cluster + PMS} - E_{cluster} - E_{PMS}$$

Where $E_{cluster + PMS}$, $E_{cluster}$ and E_{PMS} represent for the total energy of the model, the energy of the cluster model and the energy of free PMS, respectively.

The charge density difference (CDD) is calculated based on the following formula:

$$\Delta\rho = \rho(AB) - \rho(A) - \rho(B)$$

Where AB represents FeN_4+PMS, A is FeN_4, B represents PMS.

Text S3. The effect of mesoporous hollow carbon substrate on reaction activity for BPA degradation.

To demonstrate the beneficial effect of mesoporous hollow carbon substrate on reaction activity, the Fe/NC non-MCS and Fe/NC non-HMCS are employed into the system. As displayed in the **Figure S10**, only about 5% BPA can be degraded in 30 min using Fe/NC non-MCS and Fe/NC non-HMCS instead of Fe-NC HMCS. Obviously, the low SSA and lack of pore structure result in the underexposure of the active sites, while the interior active sites cannot take part in the reaction. Therefore, the Fe-NC HMCS catalyst, possessing higher surface area and numerous mesopores in hollow carbon nanospheres, is expected to be more catalytically active than Fe/NC non-MCS and Fe/NC non-HMCS catalyst. These results imply that Fe single-atom catalyst with N-doped hollow mesoporous carbon spheres is an ideal candidate catalyst for PMS activation in the AOPs.

Text S4. The possible reaction schemes for the PMS/Fe-NC HMCS system

PMS activation pathway dominated by graphitic N:

$$Graphitic\ N\ (electron\ donter) + HSO_5^- \rightarrow Graphitic\ N + SO^{\bullet}{}_4^- + OH^- \quad (1)$$

$$SO^{\bullet}{}_4^- + H_2O \rightarrow SO^2{}_4^- + H^+ + {}^{\bullet}OH \quad (2)$$

$$HSO_5^- \rightarrow SO^2{}_5^- + H^+ \quad (3)$$

$$SO^2{}_5^- + H_2O \rightarrow SO^2{}_4^- + H_2O_2 \quad (4)$$

$${}^{\bullet}OH + H_2O_2 \rightarrow HO_2^{\bullet} + H_2O \quad (5)$$

$$HO_2^{\bullet} \rightarrow O^{\bullet}{}_2^- + H^+ \quad (6)$$

$$2O^{\bullet}{}_2^- + H_2O \rightarrow {}^1O_2 + H^+ + {}^{\bullet}OH \quad (7)$$

$${}^{\bullet}OH + O^{\bullet}{}_2^- \rightarrow {}^1O_2 + OH^- \quad (8)$$

$$BPA + O^{\bullet}{}_2^- \rightarrow intermediates \rightarrow CO_2 + H_2O \quad (9)$$

PMS activation pathway dominated by Fe-N_4:

$$Fe(low\ valence)N_4 + PMS \rightarrow Fe(high\ valence)N_4 - PMS^* \quad (1)$$

$$Fe(high\ valence)N_4 - PMS^* + BPA \rightarrow intermediates \rightarrow CO_2 + H_2O \quad (2)$$

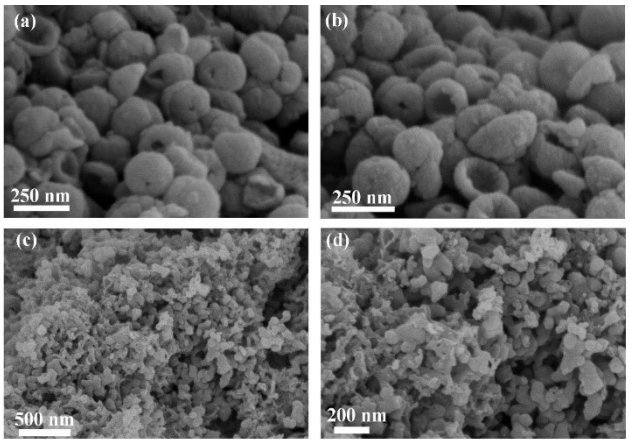

Fig. S1 (a),(b) SEM image of image of NC HMCS. (c),(d) SEM image of image of Fe NPs.

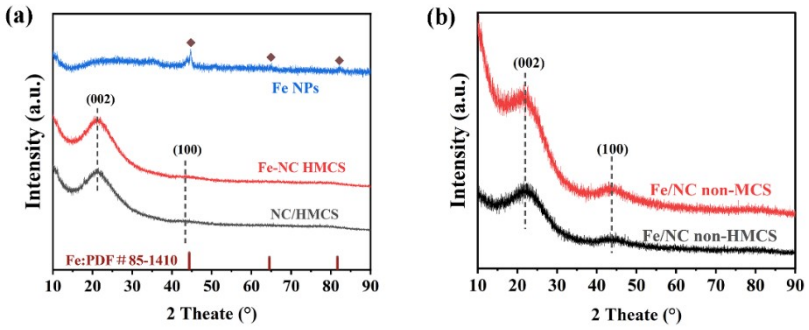

Fig. S2. (a) XRD pattens of Fe-NC HMCS, NC HMCS, Fe NPs. (b) XRD spectra of Fe/NC non-HMCS and Fe/NC non-MCS.

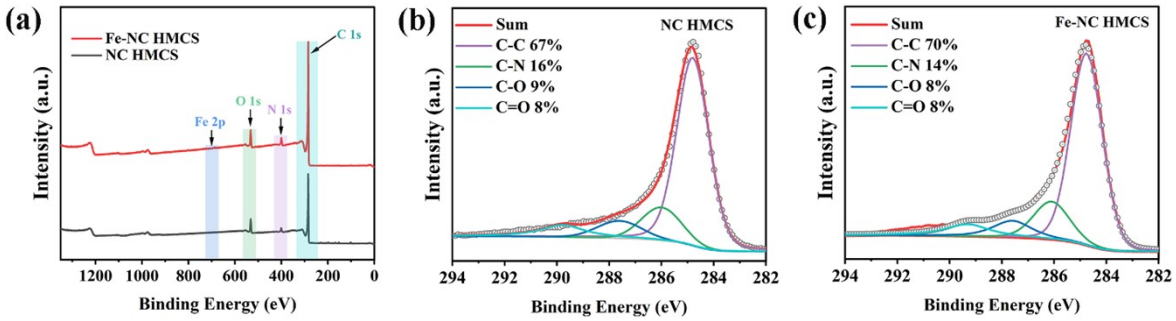

Fig. S3. (a) XPS survey spectra of Fe-NC HMCS and NC HMCS. C 1s XPS spectra of (b) NC HMCS, (c) Fe-NC HMCS, respectively.

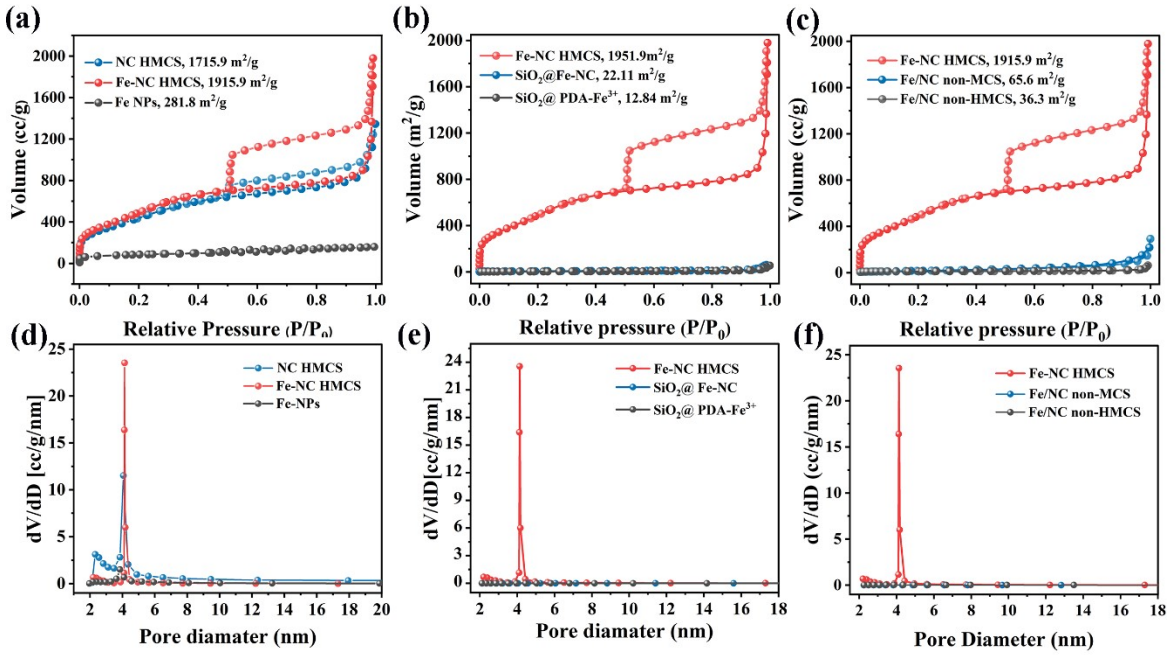

Fig. S4. (a), (b), (c) N_2 adsorption-desorption isotherms of the prepared samples. (d), (e), (f) Corresponding pore size distribution.

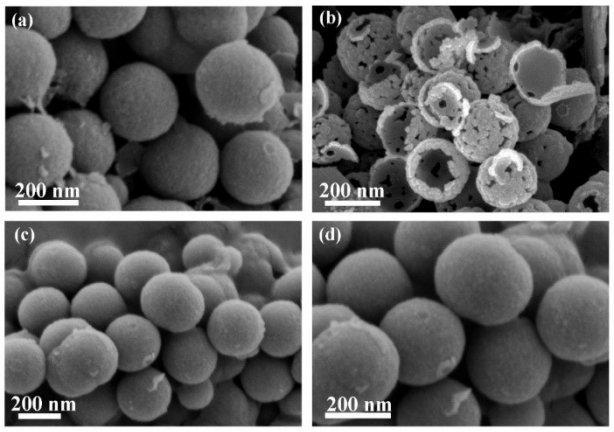

Fig. S5 (a), (b) SEM images of Fe/NC non-MCS. (c), (d) SEM images of Fe/NC non-HMCS.

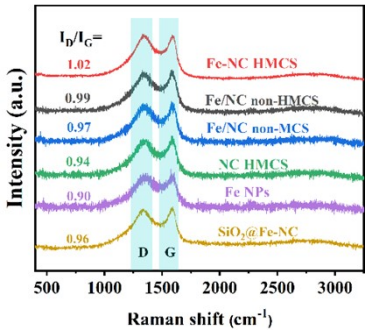

Fig. S6 Raman spectra of the prepared catalysts.

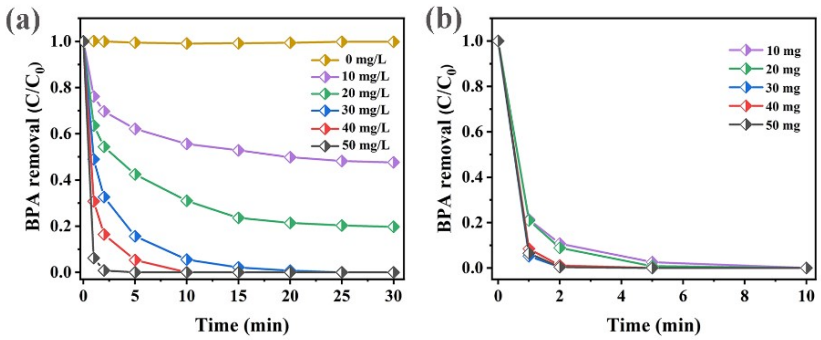

Fig. S7 Influence of (a) catalyst dosage (b) PMS dosage on BPA degradation. Reaction conditions: [BPA] = 20 ppm; [catalyst] = 0-50 mg/L; [PMS] = 10-40 mg/L; [Temp]= 25 °C; initial pH = 5.3.

The dosages of catalysts and PMS is investigated, as can be seen from the **Figure S7a** and **Figure S7b**, the enficiency of BPA removal was enhanced with increasing dosage of catalyst and PMS. therefore 50 mg/L Fe-NC HMCS was chosen to active PMS (30 mg/L) for BPA removal.

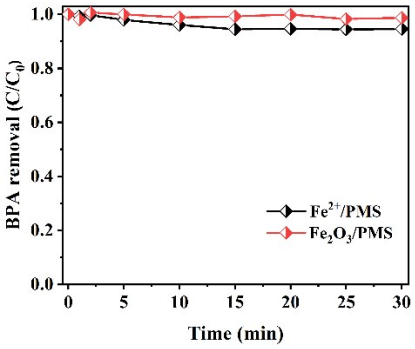

Fig. S8 Degradation of BPA by PMS activated using Fe^{2+} (Fe_2SO_4)/Fe_2O_3 as catalysts. Reaction conditions: [BPA] = 20 ppm; [catalyst] = 50 mg/L; [PMS] = 30 mg/L; [Temp]= 25 °C; initial pH = 5.3.

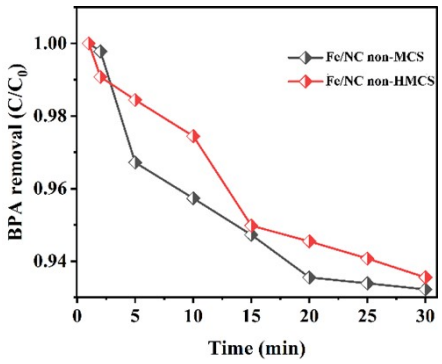

Fig. S9 Degradation of BPA by PMS activated using Fe/NC non-HMCS and Fe/NC non-MCS as catalysts. Reaction conditions: [BPA] = 20 ppm; [catalyst] = [Fe/NC non-HMCS] = [Fe/NC non-MCS] = 50 mg/L; [PMS] = 30 mg/L; [Temp]= 25 °C.

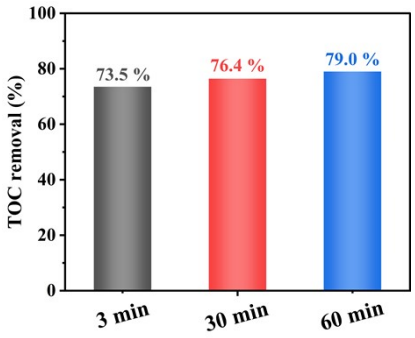

Fig. S10 TOC removal with Fe-NC HMCS as catalyst in 3min, 30min and 60 min. Reaction conditions: [BPA] = 20 ppm; [catalyst] = 50 mg/L; [PMS] = 30 mg/L; [Temp] = 25 °C; initial pH = 5.3.

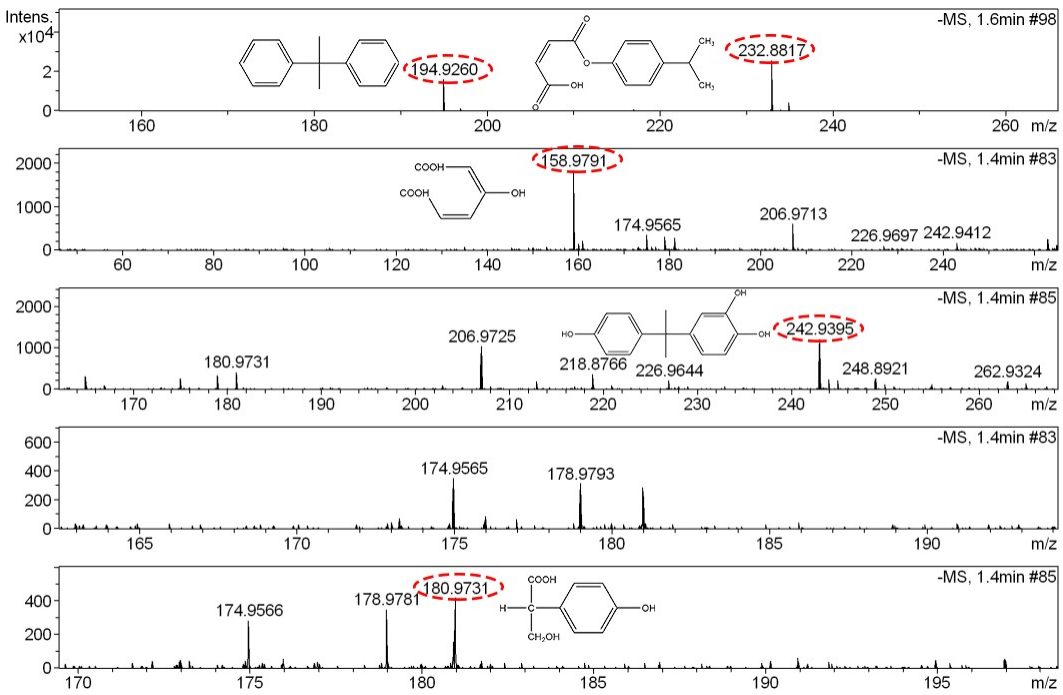

Fig. S11 The LC-MS spectra of the intermediates of BPA degradation in the PMS/Fe-NC HMCS system.

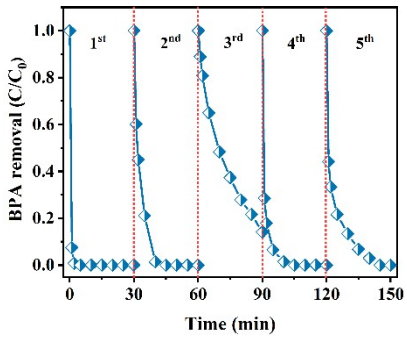

Fig. S12 Cycling tests of Fe-NC HMCS. Reaction conditions: [BPA] = 20 ppm; [catalyst] = 50 mg/L; [PMS] = 30 mg/L; [Temp] = 25 °C.

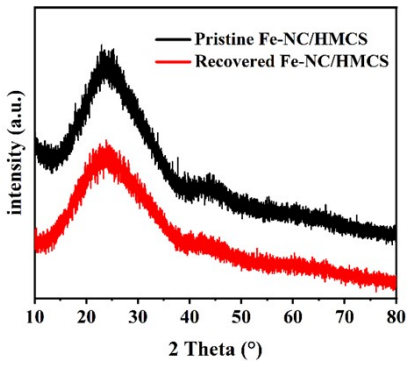

Fig. S13 (a) XRD pattens of Pristine Fe-NC HMCS and Recovered Fe-NC HMCS.

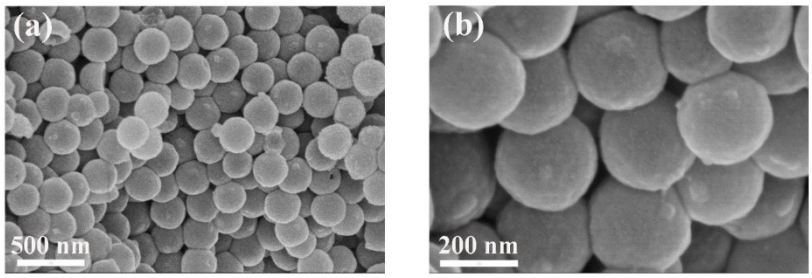

Fig. S14 (a), (b) SEM image of recovered Fe-NC HMCS.

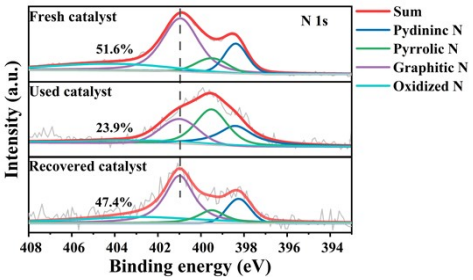

Fig. S15 The high-resolution of N 1s spectra of different nitrogen species in fresh catalyst, used catalyst and recovered catalyst, respectively.

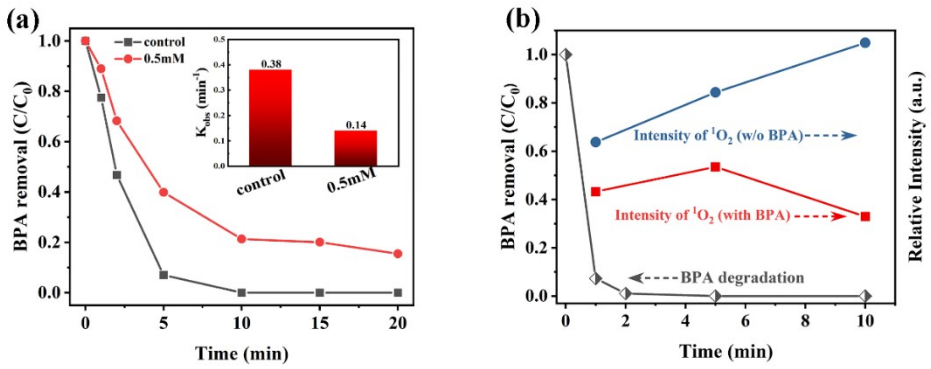

Fig. S16 (a) The effect of *β*-carotene on BPA degradation in PMS/Fe-NC HMCS system. (b) The intensity of $^1O_2$ with or without BPA. Reaction conditions: [BPA] = 20 ppm; [catalyst] = 50 mg/L; [PMS] = 30 mg/L; [*β*-carotene] = 0.5 mM; [Temp] = 25 °C; initial pH = 5.3

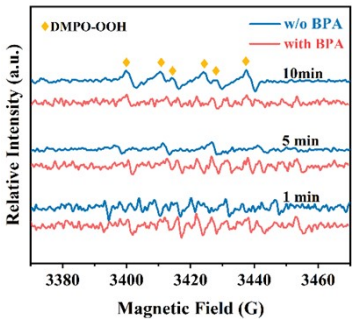

Fig. S17 EPR spectra for $O_2^{\bullet-}$ in the presence of DMPO in PMS/Fe-NC HMCS system.

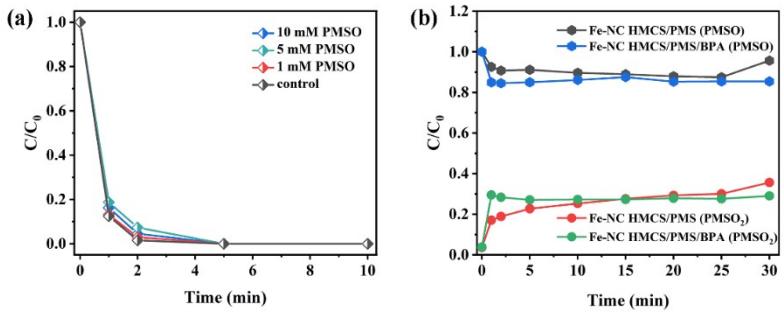

Fig. S18 (a) The effect of PMSO on BPA degradation in the PMS/Fe-NC HMCS system. (b) Decline of PMSO and production of $PMSO_2$ during the PMS/Fe-NC HMCS-coupled oxidation (with/without BPA). Reaction conditions: [BPA] = 20 ppm; [catalyst] = 50 mg/L; [PMS] = 30 mg/L; [PMSO]=1-10 mM; [Temp]= 25 °C; initial pH = 5.3.

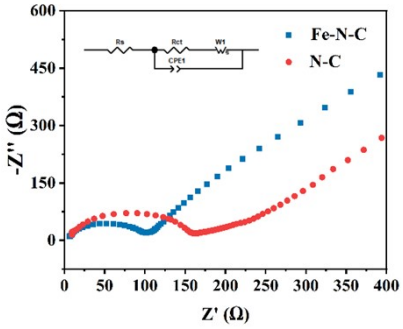

Fig. S19 EIS Nyquist plots of Fe-NC HMCS and NC HMCS. The equivalent electrical circuit image is illustrated in the inset.

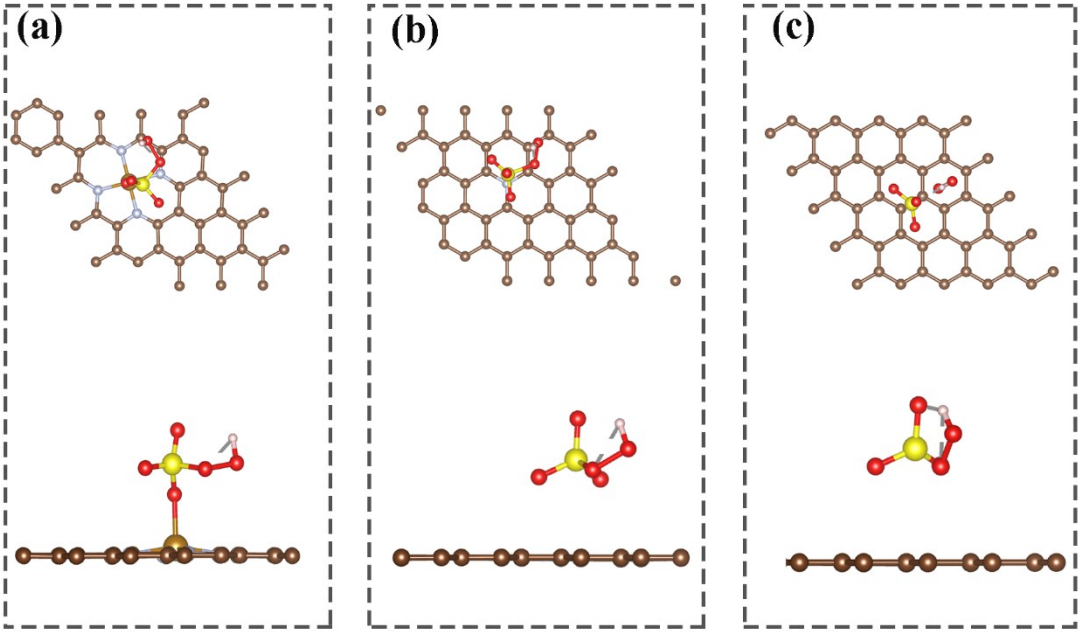

Fig. S20 Adsorption configurations of PMS on (a) Fe-NC HMCS; (b) Graphite N; (c) Carbon. (The top review is shown above, and the side review is shown below.)

Table S1. EXAFS fitting parameters at the Fe K-edge for various samples（S_0^2=0.785）

Sample	Shell	*CN*[a]	*R*(Å)[b]	σ^2(Å^2)[c]	ΔE_0(eV)[d]	*R* factor
Fe foil	Fe-Fe	8*	2.47±0.01	0.0049±0.0009	6.1	0.0067
	Fe-Fe	6*	2.85±0.01	0.0058±0.0015		
Fe_2O_3	Fe-O	6.3±1.0	1.98±0.01	0.0091±0.0018	1.4	0.0122
	Fe-Fe	6.1±0.8	2.96±0.01	0.0067±0.0008		
	Fe-Fe	4.8±0.8	3.38±0.01	0.0067±0.0008		
	Fe-Fe	6.4±1.3	3.69±0.01	0.0067±0.0008		
Sample Fe	Fe-N	4.1±0.6	2.01±0.01	0.0152±0.0022	2.7	0.0084
	Fe-C	2.0±1.1	3.06±0.01	0.0054±0.0051	10.7	

Table S2. Comparison of catalytic performance of the Fe-NC HMCS with the literature reported activators in BPA degradation. The turnover frequency (TOF) was calculated by dividing the k_{obs} by the catalyst dosage.

Activators (dosage, g L^{-1})	Pollutant (mg L^{-1})	PMS/H_2O_2/PDS (g L^{-1})	Removal efficiency	k_{obs} (min^{-1})	TOF (min^{-1})	Ref.
$CuFe_2O_4$-Fe_2O_3 (0.2)	BPA (5)	0.36	100% (10 min)	0.14	0.7	[5]
NCNTFs (0.05)	BPA (25)	0.4	97% (30 min)	0.216	4.32	[6]
FeMn-350 (0.5)	BPA (80)	0.2	100% (30 min)	0.295	0.4	[7]
NC-900 (0.2)	BPA (23)	0.6	90% (5min)	0.46	2.3	[8]
$Fe_1Mn_5Co_4$-N@C (0.1)	BPA (20)	0.2	100% (10min)	0.48	4.8	[9]
Co-N-C-900 (0.5)	BPA (80)	0.3	100% (3min)	2.81	5.62	[10]
SA Co-CN (0.02)	BPA (22)	0.03	100% (15min)	0.033	1.65	[11]
SA-Fe-NC (0.05)	BPA (23)	0.6	100% (3min)	1.99	39.8	[12]
Fe-NC HMCS (0.05)	BPA (20)	0.03	100% (5 min)	2.92	58.4	This work

Table S3. Comparison of catalytic performance of the Fe-NC HMCS with the literature reported metal-based activators in pollutant degradation. The turnover frequency (TOF) was calculated by dividing the k_{obs} by the catalyst dosage.

Activators (dosage, g L^{-1})	Metal amounts (wt.%)	Pollutant ([a] mg L^{-1}/[b] u M)	PMS/H_2O_2/PDS ([a] g L^{-1}/ [b] mM)	k_{obs} (min^{-1})	TOF (min^{-1})	Ref.
SA-Cu-NC (0.1)	3.41	BPA([a]20)	[a]0.4	0.3	3	13
CNF (0.1)	3.46	4-CP ([b]0.1)	[b]1.0	0.8	8	14
SA-CoNC (0.02)	1.6	BPA ([b]50)	[b]2.0	0.033	1.65	11
SA-Cu/rGO (0.1)	4.57	SMX ([a]10)	[a]0.4	0.406	4.06	15
SA-FeNC (0.15)	2.74	BPA ([a]20)	[a]0.4	0.24	1.6	16
1.0 SAFe-SBA(0.1)	1.01	Phenol ([a]20)	[a]1	0.05	0.5	17
SAMFe/NC (0.1)	0.81	Orange II ([b]0.65)	[a]0.10	0.133	1.33	18
Nano-Fe_3O_4 (1.0)	54	4-Chlorocatechol ([b]1000)	[b]50	2.5	2.5	19
$CoFe_2O_4$ (0.2)	73	BPA ([b]45)	[b]0.45	0.0987	0.494	20
$Mn_{1.8}Fe_{1.2}O_4$ (0.5)	79	BPA ([a]10)	[a]0.2	0.122	1.22	21
Fe_3O_4-CNTs (1)	13.6	Methylene blue ([a]0.03)	[a]1.5	0.073	0.073	22
Co_3O_4/C (0.1)	54.7	BPA ([b]87.6)	[b]325.3	0.6	6.0	23
AG/Fe_3O_4 (0.5)	86	Phenol ([b]400)	[b]240	0.021	0.042	24
AG/Fe_3O_4 (0.5)	86	2-NP ([b]400)	[b]240	0.059	0.118	24
Fe0/Fe_3C@CS (0. 2)	34.45	Phenol ([a]20)	[a]2.0	0.033	0.165	25
Fe-NC HMCS (0.05)	0.16	BPA ([a]20)	[a]0.3	2.92	58.4	This work

Table S4. Chemical components of Fe-NC HMCS (Pristine) and Fe-NC HMCS (recovered).

Samples	C, at%	N, at%	O, at%	Fe, at%
Fe-NC HMCS (fresh)	88.25	4.17	7.37	0.21
Fe-NC HMCS (recovered)	92.28	2.34	5.18	0.19

Table S5. The reaction rate constants of radicals with the corresponding scavenger

Scavenger	Targeted radicals	Rate constant (k) ($M^{-1}s^{-1}$)	Ref.
Methanol (MeOH)	$^{\bullet}OH$/ $SO_4^{\bullet-}$	9.7×10^8/ $(1.6 \sim 7.7) \times 10^7$	26
Tert-butanol (TBA)	$^{\bullet}OH$	$(3.8 \sim 7.6) \times 10^8$	27
p-benzoquinone (BQ)	$O_2^{\bullet-}$	$(0.9 \sim 1.0) \times 10^9$	28
Furfuryl alcohol (FFA)	$^1O_2$	1.2×10^8	10
β-carotene	$^1O_2$	$2 \sim 3.0 \times 10^{10}$	29

Table S6. The adsorption energy and O-O bond length of fully relaxed adsorption configurations of PMS molecule on Fe, C, CN and FeN_4.

Adsorption configurations	Adsorption energy (eV)	O–O bond length (Å)
Free PMS	--	1.331
Fe	-0.398	1.484
Carbon	-0.177	1.405
Graphitic N	-2.043	1.475
FeN_4	-1.969	1.475

References

1. Blochl, *Physical review. B, Condensed matter*, 1994, **50**, 17953-17979.
2. Kresse and Furthmuller, *Physical review. B, Condensed matter*, 1996, **54**, 11169-11186.
3. J. P. Perdew, K. Burke and M. Ernzerhof, *Physical Review Letters*, 1998, **80**, 891-891.
4. M. A. Blanco, A. M. Pendas and E. Francisco, *Journal of Chemical Theory and Computation*, 2005, **1**, 1096-1109.
5. W.-D. Oh, Z. Dong, Z.-T. Hu and T.-T. Lim, *J. Mater. Chem. A*, 2015, **3**, 22208-22217.
6. W. Ma, N. Wang, Y. Fan, T. Tong, X. Han and Y. Du, *Chem. Eng. J.,* 2018, **336**, 721-731.
7. L. Yu, G. Zhang, C. Liu, H. Lan, H. Liu and J. Qu, *Acs Catal.*, 2018, **8**, 1090-1096.
8. Y. Gao, Y. Zhu, Z. Chen, Q. Zeng and C. Hu, *Chem. Eng. J.*, 2020, **394**, 123936.
9. X. Li, Z. Ao, J. Liu, H. Sun, A. I. Rykov and J. Wang, *Acs Nano*, 2016, **10**, 11532-11540.
10. X. Cheng, H. Guo, Y. Zhang, X. Wu and Y. Liu, *Water Research*, 2017, **113**, 80-88.
11. H. Li, J. Qian and B. Pan, *Chem. Eng. J.,* 2021, **403**, 126395.
12. Y. Gao, Y. Zhu, T. Li, Z. Chen, Q. Jiang, Z. Zhao, X. Liang and C. Hu, *Environ. Sci. Technol.*, 2021, **55**, 8318-8328.
13. J. W. Pan, B. Y. Gao, P. J. Duan, K. Y. Guo, M. Akram, X. Xu, Q. Y. Yue and Y. Gao, *J. Mater. Chem. A*, 2021, **9**, 11604-11613.
14. H. Li, C. Shan and B. Pan, *Environ. Sci. Technol.*, 2018, **52**, 2197-2205.
15. F. Chen, X. L. Wu, L. Yang, C. F. Chen, H. J. Lin and J. R. Chen, *Chem. Eng. J.*, 2020, **394**, 124904.
16. Y. Li, T. Yang, S. Qiu, W. Lin, J. Yan, S. Fan and Q. Zhou, *Chem. Eng. J.*, 2020, **389**, 124382.
17. Y. Yin, L. Shi, W. Li, X. Li, H. Wu, Z. Ao, W. Tian, S. Liu, S. Wang and H. Sun, *Environ. Sci. Technol.*, 2019, **53**, 11391-11400.
18. Y. Yao, H. Yin, M. Gao, Y. Hu, H. Hu, M. Yu and S. Wang, *Chem. Eng. Sci.*, 2019, **209**, 115211.
19. J. He, X. Yang, B. Men, Z. Bi, Y. Pu and D. Wang, *Chem. Eng. J.*, 2014, **258**, 433-441.
20. S. Yang, X. Qiu, P. Jin, M. Dzakpasu, X. C. Wang, Q. Zhang, L. Zhang, L. Yang, D. Ding, W. Wang and K. Wu, *Chem. Eng. J.*, 2018, **353**, 329-339.
21. G.-X. Huang, C.-Y. Wang, C.-W. Yang, P.-C. Guo and H.-Q. Yu, *Environ. Sci. Technol.*, 2017, **51**, 12611-12618.
22. A. Tolba, M. G. Alalm, M. Elsamadony, A. Mostafa, H. Afify and D. D. Dionysiou, *Process Saf. Environ. Prot.*, 2019, **128**, 273-283.
23. M. A. N. Khan, P. K. Klu, C. Wang, W. Zhang, R. Luo, M. Zhang, J. Qi, X. Sun, L. Wang and J. Li, *Chem. Eng. J.*, 2019, **363**, 234-246.
24. P. K. Boruah, B. Sharma, I. Karbhal, M. V. Shelke and M. R. Das, *J. Hazard. Mater.*, 2017, **325**, 90-100.
25. Y. Wang, H. Sun, X. Duan, H. M. Ang, M. O. Tade and S. Wang, *Appl. Catal., B*, 2015, **172**, 73-81.

1. Blochl, *Physical review. B, Condensed matter*, 1994, **50**, 17953-17979.
2. Kresse and Furthmuller, *Physical review. B, Condensed matter*, 1996, **54**, 11169-11186.
3. J. P. Perdew, K. Burke and M. Ernzerhof, *Physical Review Letters*, 1998, **80**, 891-891.
4. M. A. Blanco, A. M. Pendas and E. Francisco, *Journal of Chemical Theory and Computation*, 2005, **1**, 1096-1109.

5. W.-D. Oh, Z. Dong, Z.-T. Hu and T.-T. Lim, *Journal of Materials Chemistry A*, 2015, **3**, 22208-22217.
6. W. Ma, N. Wang, Y. Fan, T. Tong, X. Han and Y. Du, *Chemical Engineering Journal*, 2018, **336**, 721-731.
7. L. Yu, G. Zhang, C. Liu, H. Lan, H. Liu and J. Qu, *Acs Catalysis*, 2018, **8**, 1090-1096.
8. Y. Gao, Y. Zhu, Z. Chen, Q. Zeng and C. Hu, *Chemical Engineering Journal*, 2020, **394**, 123936.
9. X. Li, Z. Ao, J. Liu, H. Sun, A. I. Rykov and J. Wang, *Acs Nano*, 2016, **10**, 11532-11540.
10. X. Cheng, H. Guo, Y. Zhang, X. Wu and Y. Liu, *Water Research*, 2017, **113**, 80-88.
11. H. Li, J. Qian and B. Pan, *Chemical Engineering Journal*, 2021, **403**, 126395.
12. Y. Gao, Y. Zhu, T. Li, Z. Chen, Q. Jiang, Z. Zhao, X. Liang and C. Hu, *Environmental science & technology*, 2021, **55**, 8318-8328.
13. J. W. Pan, B. Y. Gao, P. J. Duan, K. Y. Guo, M. Akram, X. Xu, Q. Y. Yue and Y. Gao, *Journal of Materials Chemistry A*, 2021, **9**, 11604-11613.
14. H. Li, C. Shan and B. Pan, *Environmental Science & Technology*, 2018, **52**, 2197-2205.
15. F. Chen, X. L. Wu, L. Yang, C. F. Chen, H. J. Lin and J. R. Chen, *Chemical Engineering Journal*, 2020, **394**, 124904.
16. Y. Li, T. Yang, S. Qiu, W. Lin, J. Yan, S. Fan and Q. Zhou, *Chemical Engineering Journal*, 2020, **389**, 124382.
17. Y. Yin, L. Shi, W. Li, X. Li, H. Wu, Z. Ao, W. Tian, S. Liu, S. Wang and H. Sun, *Environmental Science & Technology*, 2019, **53**, 11391-11400.
18. Y. Yao, H. Yin, M. Gao, Y. Hu, H. Hu, M. Yu and S. Wang, *Chemical Engineering Science*, 2019, **209**, 115211.
19. J. He, X. Yang, B. Men, Z. Bi, Y. Pu and D. Wang, *Chemical Engineering Journal*, 2014, **258**, 433-441.
20. S. Yang, X. Qiu, P. Jin, M. Dzakpasu, X. C. Wang, Q. Zhang, L. Zhang, L. Yang, D. Ding, W. Wang and K. Wu, *Chemical Engineering Journal*, 2018, **353**, 329-339.
21. G.-X. Huang, C.-Y. Wang, C.-W. Yang, P.-C. Guo and H.-Q. Yu, *Environmental Science & Technology*, 2017, **51**, 12611-12618.
22. A. Tolba, M. G. Alalm, M. Elsamadony, A. Mostafa, H. Afify and D. D. Dionysiou, *Process Safety and Environmental Protection*, 2019, **128**, 273-283.
23. M. A. N. Khan, P. K. Klu, C. Wang, W. Zhang, R. Luo, M. Zhang, J. Qi, X. Sun, L. Wang and J. Li, *Chemical Engineering Journal*, 2019, **363**, 234-246.
24. P. K. Boruah, B. Sharma, I. Karbhal, M. V. Shelke and M. R. Das, *Journal of Hazardous Materials*, 2017, **325**, 90-100.
25. Y. Wang, H. Sun, X. Duan, H. M. Ang, M. O. Tade and S. Wang, *Applied Catalysis B-Environmental*, 2015, **172**, 73-81.
26. L. Wang, X. Lan, W. Peng and Z. Wang, *Journal of hazardous materials*, 2020, 124436-124436.
27. L. Zhang, Y. Nie, C. Hu and X. Hu, *Journal of Hazardous Materials*, 2011, **190**, 780-785.
28. Y. Zhou, S. Fang, M. Zhou, G. Wang, S. Xue, Z. Li, S. Xu and C. Yao, *Journal of Alloys and Compounds*, 2017, **696**, 353-361.
29. Y. Gao, Z. Chen, Y. Zhu, T. Li and C. Hu, *Environmental Science & Technology*, 2020, **54**, 1232-1241.